



1 Gridded maps of geological methane emissions and their isotopic signature

2

3 Giuseppe Etiope^{1,2}, Giancarlo Ciotoli^{3,1}, Stefan Schwietzke⁴, Martin Schoell⁵

4

5 ¹ Istituto Nazionale di Geofisica e Vulcanologia, Roma Italy6 ² Faculty of Environmental Science and Engineering, Babes Bolyai University, Cluj-Napoca, Romania7 ³ Istituto di Geologia Ambientale e Geoingegneria, CNR-IGAG, Roma, Italy8 ⁴ Cooperative Institute for Research in Environmental Sciences, University of Colorado, Boulder, Colorado, USA, and NOAA Earth
9 System Research Laboratory, Global Monitoring Division, Boulder, Colorado, USA.10 ⁵ Gas-Consult Int., Pleasanton, California, USA

11

12 Correspondence to: Giuseppe Etiope (giuseppe.etiope@ingv.it)

13

14

15 Abstract

16 Methane (CH₄) is a powerful greenhouse gas, whose natural and anthropogenic emissions contribute ~20% to global
17 radiative forcing. Its atmospheric budget (sources and sinks), however, has large uncertainties. Inverse modelling, using
18 atmospheric CH₄ trends, spatial gradients and isotopic source signatures, has recently improved the major source
19 estimates and their spatial-temporal variation. Nevertheless, isotopic data lack CH₄ source representativeness for many
20 sources, and CH₄ source attribution is affected by incomplete knowledge of the spatial distribution of some sources,
21 especially those related to fossil (radiocarbon-free) and microbial gas. This gap is particularly wide for geological CH₄
22 seepage, i.e., the natural degassing of hydrocarbons from the Earth's crust. While geological seepage is widely
23 considered the second most important natural CH₄ source after wetlands, it has been mostly neglected in top-down CH₄
24 budget studies, partly given the lack of detailed a priori gridded emission maps. Here, we report for the first time global
25 gridded maps of geological CH₄ sources, including emission and isotopic data. The 1°x1° maps include the four main
26 categories of natural geo-CH₄ emission: (a) onshore hydrocarbon macro-seeps, including mud volcanoes, (b) submarine
27 (offshore) seepage, (c) diffuse microseepage and (d) geothermal manifestations. An inventory of point sources and area
28 sources was developed for each category, defining areal distribution (activity), CH₄ fluxes (emission factors) and its
29 stable C isotope composition (δ¹³C-CH₄). These parameters were determined considering geological factors that control
30 methane origin and seepage (e.g., petroleum fields, sedimentary basins, high heat flow regions, faults, seismicity). The
31 global geo-source map reveals that the regions with the highest CH₄ emissions are all located in the northern
32 hemisphere, in North America, the Caspian region, Europe, and in the East Siberian Arctic Shelf. The globally gridded
33 CH₄ emission estimate (37 Tg year⁻¹ exclusively based on data and modeling specifically targeted for gridding, and 43-
34 50 Tg year⁻¹ when extrapolated to also account for onshore and submarine seeps with no location specific
35 measurements available) is compatible with published ranges derived by top-down and bottom-up procedures. Improved
36 activity and emission factor data allowed to refine previously published mud volcanoes and microseepage emission
37 estimates. The emission-weighted global mean δ¹³C-CH₄ source signature of all geo-CH₄ source categories is -48.5‰ to
38 -49.4‰. These values are significantly lower than those attributed so far in inverse studies to fossil fuel sources (-44‰)
39 and geological seepage (-38‰). It is expected that using these updated more ¹³C-depleted, isotopic signatures in
40 atmospheric modelling will increase the top-down estimate of the geological CH₄ source. The geo-CH₄ emission grid
41 maps can now be used to improve atmospheric CH₄ modeling, thereby improving the accuracy of the fossil fuel and
42 microbial components. Grid csv files are available at <https://doi.org/10.25925/4j3f-he27>.



1

2 **1. Introduction**

3 Methane (CH₄) is a powerful greenhouse gas, whose concentrations in the atmosphere increased about 2.5
4 times since the pre-industrial era (1750), approaching 1.9 ppm in 2018. With a global emission of about 550
5 Tg CH₄ year⁻¹ (Kirschke et al., 2013), CH₄ contributes ~20% to global radiative forcing (Ciais et al. 2013).
6 The CH₄ budget, i.e. natural and anthropogenic sources and sinks, estimated by either bottom-up (emission
7 inventories) or top-down (inverse modelling) approaches (e.g., Saunio et al., 2016 and Refs. therein), is
8 subject to considerable uncertainties, however. Top-down estimates show strong disagreement with bottom-
9 up estimates, both globally and regionally. Three-dimensional (3D) inversion modelling, using trends, spatial
10 gradients and isotopic measurements (stable C isotope ratio, δ¹³C-CH₄) of source signatures and the
11 atmosphere, recently improved the knowledge of major sources (fossil-fuel, agriculture and wetlands) and
12 their spatio-temporal variation (e.g., Schwietzke et al 2016). Nevertheless, isotopic data lack
13 representativeness of CH₄ source signatures for many sources, and source attributions are limited by
14 incomplete knowledge of the spatial distribution of some major sources, especially fossil fuel and microbial.
15 In this respect, geological CH₄ emissions, i.e. the natural component of fossil fuel (¹⁴C-free) emission, play a
16 critical role. Geological CH₄ sources are the natural degassing of hydrocarbons from the Earth's crust (e.g.,
17 Etiope and Klusman, 2002; Kvenvolden and Rogers, 2005; Etiope, 2015). Geo-CH₄ originated in deep rocks
18 by biotic (i.e. microbial and thermogenic) processes related to petroleum fields in sedimentary basins, as
19 described in a wide petroleum geology literature (see for example Etiope, 2017 for a recent overview).
20 Relatively minor amounts of CH₄ can also be produced by abiotic processes, which do not involve organic
21 matter in rocks (e.g., magma degassing, high temperature post-magmatic process, CO₂ hydrogenation or
22 Sabatier reaction, in geothermal/volcanic systems and ultramafic igneous rocks; e.g., Etiope and Sherwood
23 Lollar, 2013). Surface emissions of geological CH₄ occur through the process known as "gas seepage",
24 which includes point sources (gas-oil seeps, mud volcanoes, springs, geothermal manifestations) and area
25 sources (diffuse "microseepage"). Once considered a minor natural CH₄ source globally (e.g., Lelieveld et
26 al., 1998; Prather et al., 2001), geological degassing is today recognised as the second most important
27 natural CH₄ source after wetlands, as indicated by the agreement between bottom-up and top-down
28 estimates converging to 40-60 Tg year⁻¹ (Etiope et al. 2008; Ciais et al. 2013; Etiope, 2015; Schwietzke et al.
29 2016). Nevertheless, geological seepage has mostly been neglected in global top-down CH₄ budget studies
30 (e.g., Bousquet et al. 2006; Bergamaschi et al. 2014). In addition, geological CH₄ has erroneously been
31 considered to be typically ¹³C-enriched, thus with relatively high δ¹³C-CH₄ values compared to biological
32 sources such as wetlands (a global average of -38‰ was assumed for seepage by Sapart et al. 2012). In
33 petroleum geochemistry it is well known, in fact, that in addition to the common thermogenic gas produced
34 by moderate to high maturity source rocks, typically with δ¹³C-CH₄ from -30‰ to about -50‰, vast amounts
35 of methane in sedimentary basins are microbial (thus with δ¹³C-CH₄ ranging from -55 to about -90‰) and
36 thermogenic from low maturity source rocks, with δ¹³C-CH₄ from -50‰ to about -70‰ (Etiope, 2017; Milkov
37 and Etiope, 2018). Degassing (seepage) to the atmosphere of ¹³C-depleted geo-CH₄ sources is also widely
38 documented (e.g., Etiope et al. 2009 and references therein). In addition to using unrepresentatively heavy
39 δ¹³C-CH₄ geo-CH₄ values in previous studies, detailed a priori gridded maps of geo-CH₄ emissions and its



1 isotopic signatures, which are essential for 3D inverse modeling and to discriminate between natural and
2 anthropogenic microbial emissions, are currently lacking.

3 Here, we report the first global grid maps of geological CH₄ sources, including emissions and isotopic source
4 signatures. The maps, elaborated by ArcGIS at 1°×1° resolution, include the four main categories of natural
5 geological CH₄ sources: (a) onshore hydrocarbon macro-seeps (including mud volcanoes), (b) submarine
6 (offshore) seeps, (c) diffuse microseepage and (d) geothermal manifestations. For each category we have
7 developed an inventory of point sources and area sources, including coordinates (areal distribution, i.e.
8 activity), estimated CH₄ fluxes (emission factors) and δ¹³C-CH₄ values. These parameters have been
9 determined considering several geological factors that control CH₄ origin and seepage (petroleum fields,
10 sedimentary basins, faults, earthquakes, geothermal/volcanic systems), based on published and originally
11 *ad-hoc* developed datasets. Integrated (total geo-CH₄) maps and associated text files (csv, comma-
12 separated-values) have been generated to facilitate atmospheric CH₄ modeling to improve the accuracy of
13 fossil fuel and microbial components. Gridded geo-CH₄ emissions were compared with published global
14 estimates, derived by different approaches (e.g., Etiope et al. 2008; Etiope, 2012; 2015; Schwietzke et al.
15 2016). In particular, the gridding implied a careful assessment of the spatial distribution and emission factors
16 for mud volcanoes and microseepage, thus allowing for new bottom-up estimates of their global emissions.

17

18

19 **2. Classification of the geological CH₄ sources**

20 Geological CH₄ sources can be classified into four major categories:

21 (a) Onshore hydrocarbon seeps (or macro-seeps) in sedimentary (petroliferous) basins including CH₄-rich
22 gas-oil seeps, mud volcanoes (MV) and gas-bearing springs. Hereafter referred as **OS**.

23 (b) Submarine (offshore) seeps, where CH₄ released from shallow seafloor (coastal areas or shelves,
24 generally up to 300-400 m below sea level) can cross the water column and enter the atmosphere. Hereafter
25 referred as **SS**.

26 (c) Diffuse microseepage in sedimentary (petroliferous) basins, the widespread, invisible exhalation of CH₄
27 typically detected in correspondence with gas-oil fields. Hereafter referred as **MS**.

28 (d) Geothermal and volcanic manifestations, where CH₄ is a minor component (subordinated to CO₂) but
29 with potentially significant fluxes to the atmosphere. Hereafter referred as **GM**.

30 These “geo-methane” sources are extensively described and discussed in a wide body of literature; for
31 details the reader may refer to Etiope and Klusman (2002); Judd (2004); Kvenvolden and Rogers (2005);
32 McGinnis et al (2006); Etiope et al. (2007); Judd and Hovland (2007); Etiope et al. (2008); Etiope and
33 Klusman (2010); Etiope (2015), Mazzini and Etiope (2017). Their global bottom-up and top-down emissions,
34 compared with other natural CH₄ sources, are summarized in Fig. 1.

35

36

37 **3. Methodology**

38 Methods for creating CH₄ emission and δ¹³C-CH₄ grids vary by geo-CH₄ category, based on the data
39 availability and specific seepage characteristics. Methods are therefore described in detail for each category



1 in Sections 4 (OS), 5 (SS), 6 (MS) and 7 (GM). First, a brief overview of the different types of input data and
2 gridding procedure is given below.

3

4 **3.1 Data sources**

5 Table 1 summarizes how the four categories of geo-CH₄ sources were elaborated, showing data sources,
6 the parameters used to define the “activity” (spatial distribution), the “emission factors” (fluxes), and the
7 attribution of the isotopic CH₄ values. The list and web links of the sources of databases are reported in the
8 Supplement.

9

10 **3.2. Gridding procedure**

11 The gridding procedure is the same for each geo-CH₄ source category. Geo-CH₄ emission and isotope
12 datasets were imported in ArcGIS environment and saved in shapefile format. A 1°x1° vector (polygon)
13 square grid was then created as a base for all map calculations. The grid was then joined with single OS,
14 SS, MS, GM shapefiles. The final csv files include data fields that define the coordinates of each cell
15 centroid, the variable name and its unit of measurement (tonnes year⁻¹ per cell for CH₄ emission and ‰ for
16 δ¹³C-CH₄, according to VPDB, Vienna Pee Dee Belemnite, standard). For the grid cell values, the number
17 zero (0) is used to indicate an actual or best emission estimate of zero (no seepage), whereas -9999
18 indicates lack of knowledge, of the emission. Specifically:

19 In the CH₄ output files:

20 - zero (0) value is used for:

- 21 - all offshore cells of the onshore seepage shape files (OS, MS and GM)
- 22 - all onshore cells of the offshore seepage (SS).
- 23 - all onshore cells outside the potential MS area
- 24 - onshore cells without OS or GM sources
- 25 - offshore cells outside the SS areas

26 - the number -9999 is used for:

- 27 - cells within SS areas where emissions are unknown.

28 The categories OS, MS and GM, due to the method of emission derivation (see related sections below) have
29 always an emission value.

30 In the isotope files:

- 31 - an isotopic value is reported in each cell that has a flux value;
- 32 - where specific values are not available (as occurred in OS and SS), the global weighted average δ¹³C for
33 the relative emission category is reported;
- 34 - four decimals are used for global weighted average isotope values; this can help to trace back which cells
35 are based on cell-specific data (with one decimal), and which contain weighted averages (four decimals);
- 36 - the value -9999 is used only for cells with no emissions in the corresponding CH₄ output files.

37 The application of such rules is described in the specific chapters of the four emission categories. Once
38 individual OS, SS, MS, GM maps/files were produced, they were merged into a unified, total geo-CH₄
39 gridding: emissions per cell were summed and δ¹³C values were averaged.



1

2 **4. Onshore seeps (OS)**

3

4 **4.1 Global seep count and distribution**

5 The spatial distribution (activity) of onshore seeps is derived from geographic coordinates of 2827 seeps,
6 from 89 countries, reported in a global onshore seep dataset, which includes 1119 oil seeps, 846 gas seeps,
7 741 mud volcanoes and 121 gas-bearing springs. This dataset is an updated version of a previous inventory
8 (named GLOGOS, reporting 2100 seeps) available from CGG (2015) and described in Etiope (2015). The
9 global distribution of OS is reported in Fig. 2.

10 The seeps listed in the dataset generally refer to individual focused vents (single macro-seep
11 manifestations) but in several cases they refer to groups or clusters, or even wide zones of multiple seep
12 points. 612 seeps (569 gas-oil seeps and 43 mud volcanoes) could not be geographically located with
13 precision and they are listed without coordinates (in addition to the 2827 seeps). The dataset, therefore,
14 actually mentions a total of 3439 seeps or seepage sites, including 3396 gas-oil seeps and 784 mud
15 volcanoes. The total number of 3439 OS represents about 30% of total seeps assumed to exist on Earth
16 ($\approx 10,000$ was proposed by Clarke and Cleverly, 1991), but the present dataset includes the largest and
17 more active seeps (especially for MV) because they are more easily documented and have attracted
18 attention for scientific research, petroleum exploration, and natural heritage protection. Small or inactive
19 seeps tend to be less observed and reported. In particular, the MV inventory is almost complete, probably
20 missing smaller MVs in Asia. The gas-oil seeps in the dataset likely contribute more than 50% of the
21 previously estimated total gas-oil seep emission. Africa and South America likely host a large number of
22 gas-oil seeps and springs not documented in the dataset.

23

24

25 **4.2 Attribution of CH₄ emissions to individual seeps**

26 The attribution of CH₄ emission magnitudes to individual seep locations follows two different approaches for
27 (a) gas-oil seeps or springs and (b) mud volcanoes (MV).

28

29 **4.2.1 Emission of gas-oil seeps and springs**

30 Direct measurements of CH₄ flux are available for only a few tens of gas-oil seeps in Europe, Asia and North
31 America. In general, therefore, potential or theoretical flux values have been attributed to the inventoried
32 seeps. Theoretical emission values can be reasonably provided only in terms of order of magnitude (i.e. 10⁰,
33 10¹, 10², 10³, 10⁴ tonnes year⁻¹). For gridding purposes, however, theoretical values (approximate working
34 values) were used taking into account basic characteristics of the several seeps, i.e. the type of seep (for
35 example, gas seeps generally release more methane than oil seeps), the activity and size of the seep
36 (according to specific literature, reports, web images), and taking into account, as "calibration", experimental
37 data, i.e., flux values measured in the field from seeps covering a wide range of activity and size. The
38 theoretical values also take into account the gas emission from the invisible miniseepage, which surrounds
39 the macro-seep vent, and which adds an amount of gas that may be three times higher than that released



1 from the vents (Etiopie, 2015). This resulted in the attribution of the values reported in Table S1 in the
2 Supplement. These values should be considered as first-order estimates and care should be taken when
3 using individual seep flux estimates from this product to derive global emission estimates, as discussed in
4 section 4.5.

5

6 *4.2.2 Emission of mud volcanoes (MV)*

7 For MV, emission values refer to the continuous quiescent degassing, i.e. they do not include emissions
8 during episodic eruptions, as these are practically impossible to estimate for each MV. Eruptions were
9 considered separately for the global emission estimate as discussed below. The quiescent emissions were
10 attributed to each MV following the activity (area) and emission factor approach as follows.

11 A precise evaluation of the MV areas was performed by accurate image (Google Earth) analysis. For each
12 MV visible on Google Earth images, the area of the entire MV structure, including central craters and flanks,
13 was estimated by drawing a polygon encompassing the mud cover and mound flanks. For smaller MV, not
14 visible on low resolution Google Earth images or covered by vegetation, photos or information from
15 published literature or web sources were considered to define the order of magnitude of the MV size. The
16 global MV area resulted to be about 680 km².

17 The MV emissions were then assessed using an updated dataset of fluxes measured from 16 MV in
18 Azerbaijan, Romania, Italy, Taiwan, China and Japan (Table S2 in Supplement), distinguishing between the
19 macro-seepage (the focused emission from craters and vents) and miniseepage (the diffuse degassing from
20 the ground surrounding craters and vents). Regression analysis between MV area, miniseepage and macro-
21 seep flux of these measured MV was used to derive miniseepage and macro-seep flux (and thus the total
22 CH₄ emission) for each MV of the inventory, whose area was determined as previously indicated. The
23 procedure is described in detail in the Supplement (Section S1.1)

24

25 *4.2.3 The "big emitters"*

26 OS with emissions in the order of 10⁴ t CH₄ year⁻¹ (i.e. that may emit at least 10,000 tonnes CH₄ year⁻¹
27 individually) add up to 76, and they can be considered "big emitters"; they typically refer to large, very active
28 and frequently erupting MVs and gas burning seeps. The 76 big emitters likely dominate the spatial
29 distribution of CH₄ emissions (they represent 63% of the total OS emission) and the weighted global mean
30 isotopic value. As shown in Fig. 3, it is clear that, on a global scale, the Caspian and Mid-East regions
31 represent the main OS output areas.

32

33

34 **4.3 Attribution of the $\delta^{13}\text{C-CH}_4$ value**

35 For each seep the $\delta^{13}\text{C-CH}_4$ value is:

36 (a) measured, as indicated in the literature, or (b) estimated on the basis of isotopic values

37 - of similar seeps occurring in the same basin

38 - of reservoir gas in the same petroleum field, from Sherwood et al. (2017) dataset or literature

39 - suggested by local petroleum geology (existence of microbial gas, thermogenic gas, oil).



1 The OS emission-weighted value (Section 4.5.2) was used for gridding where the isotopic value could not be
2 assessed. The global distribution of three classes of $\delta^{13}\text{C-CH}_4$ value is shown in Fig. S4 in the Supplement.

3

4

5 **4.4 OS gridding**

6 The OS shapefile generated in ArcGIS was spatially joined to the $1^\circ \times 1^\circ$ vector square grid. OS occur in 616
7 cells, for a total emission of 3.87 Tg/y (Fig. 4). This is about 0.07 Tg/y higher than the actual sum of the seep
8 emission in the inventory because of multiple counting of 57 seeps that occur exactly on the boundary of a
9 cell.

10

11

12 **4.5 Evaluation of global OS emission and $\delta^{13}\text{C-CH}_4$**

13

14 **4.5.1 Re-assessing global OS emission**

15 Because of the large uncertainty of the theoretical values of flux data considered for individual oil-gas seeps
16 in the OS inventory, the OS flux grids are not meant to update or refine the previous global OS CH_4 emission
17 estimate (Etiopie et al. 2008). A comparison with the published bottom-up estimates can establish whether
18 the OS inventory data used in the OS flux grids are plausible. However, the procedure developed to attribute
19 CH_4 emissions to MVs can represent a refinement of the global MV emission estimate.

20 Published bottom-up estimates of CH_4 emission from onshore macro-seeps are reported in Table 2. Some
21 estimates included shallow submarine MV (e.g., Dimitrov, 2003; Milkov et al. 2003), which must be
22 considered within the category SS in this work. Therefore, those estimates are indicated in the table as
23 upper limit. Because the data of the OS inventory, as explained in Section 4.2, refer only to quiescent
24 degassing, the table distinguishes emissions that exclude MV eruptions (quiescent degassing) and those
25 that include MV eruptions.

26 Concerning gas-oil seeps and springs, the use of the theoretical values, as described in Section 4.2, results
27 in global CH_4 emission of about 1 Tg/y (Table 2). As indicated in Section 4.1, the OS dataset, although
28 representing only 30% of all seeps existing on Earth, includes the largest and more active seeps, which may
29 contribute at least 50% of the global emission; accordingly, the total gas-oil seep emission could be likely
30 around 2 Tg/y. Any further or more detailed extrapolation to a global seep emission estimate would be
31 inappropriate.

32 The global MV emission from quiescent degassing, i.e. the sum of the MV emission values reported in the
33 OS dataset, amounts to 2.83 Tg year⁻¹. The total CH_4 emissions from the 2827 OS seeps is, therefore, about
34 3.8 Tg year⁻¹ (1 + 2.8 Tg year⁻¹). The OS-MV dataset likely represents about 90% of total MVs assumed to
35 exist on Earth (≈ 900 ; Dimitrov, 2002; Etiopie and Milkov, 2004); extrapolating to the total MV number would
36 result in a global MV emission of approximately 3 Tg year⁻¹. This is within the range suggested by Etiopie
37 and Milkov (2004). Compared to previous emission estimates of Etiopie and Milkov (2004) and Etiopie et al
38 (2011), the present MV estimate used a lower activity, i.e. lower global area, 680 km² instead of 2800 km²
39 (which was suggested by data provided by Azerbaijan Geological Institute) but relatively higher emission



1 factors. Concerning the MV eruptions, we can only use, again, the rough estimations indicated in Dimitrov
2 (2003), Milkov et al. (2003) and Aliyev et al. (2012) (i.e., average gas flux during eruptions of MVs in
3 Azerbaijan $2.5 \times 10^8 \text{ m}^3$, the proportions of eruptive MVs: 27%, and the frequency of eruption: 1.35
4 eruptions/year), which translate into a total eruptive emission of 3.1 Tg year^{-1} (Milkov et al. 2003). Therefore,
5 the global OS emission, including MV eruptions and assuming the theoretical values for the gas-oil seeps
6 and springs, would be $\sim 8.1 \text{ Tg year}^{-1}$, which is within 10% of the lower range proposed by Etiope et al.
7 (2008).

8

9 4.5.2 The average emission-weighted $\delta^{13}\text{C-CH}_4$

10 The total mean value of $\delta^{13}\text{C-CH}_4$ from all OS is -47.8‰ , and that from the 76 big emitters is -46.7‰ . The
11 global OS emission-weighted mean value of $\delta^{13}\text{C-CH}_4$ is -46.6‰ .

12

13

14 4.6 OS uncertainties

15 *Spatial distribution uncertainty:* In the $1^\circ \times 1^\circ$ grid, the uncertainty of the geographic distribution of the OS is
16 practically zero, as all identified seeps have geographic coordinates within an error $< 1^\circ$.

17 *Emission uncertainty:* The modeled emission values attributed to the seeps/springs take into account basic
18 seep characteristics including the type of seep, the activity and size of the seep, and experimental data from
19 some seeps (see section 4.2.1), and can be considered only in terms of order of magnitude. The uncertainty
20 is therefore also in terms of order of magnitude. The uncertainty of the emission values attributed to MVs
21 depends on the representativeness of the average emission factors (i.e. the equation in the regression lines
22 of Fig. S2 and S3) and the areas estimated (see Supplement).

23 *$\delta^{13}\text{C-CH}_4$ uncertainty:* The uncertainty of measured $\delta^{13}\text{C}$ values (from literature) practically corresponds to
24 laboratory analytical uncertainty (typically $< 0.1\text{‰}$). The maximum uncertainty of the estimated $\delta^{13}\text{C}$ values
25 (based on criteria described in Section 4.3) is approximately within 15‰ , i.e. half of the range of $\delta^{13}\text{C}$ values
26 for typical microbial (-80 to -60‰) and thermogenic (-50 to -20‰) gas. The uncertainty of the emission-
27 weighted mean (-46.6‰) is mainly induced by the 76 big emitters, for which the $\delta^{13}\text{C}$ values are available or
28 estimated with good approximation, leading to a mean value of -46.7‰ .

29

30

31 5. Submarine seepage (SS)

32

33 5.1 Assessment of global SS area

34 A specific dataset of offshore seepage areas, in coastal regions and shallow seas (typically $< 500 \text{ m}$ deep,
35 which is generally the maximum depth of seeps that may affect the atmosphere; e.g., McGinnis et al. 2006),
36 was developed based on available literature (Table S4 in the Supplement). The dataset includes:

37 a) Submarine seeps where gas was observed to reach the sea surface via bubble plumes and the output to
38 the atmosphere was estimated: flux emission estimates are available from 15 zones (from focused, point-



1 source, manifestations to wide regional areas) in the seas of Australia, Bulgaria, Brunei, California, Canada,
2 Chile, China, Denmark, Georgia, Greece, Norway, Spain, Romania, Russia, Turkey, Ukraine, United
3 Kingdom, USA.

4 b) Submarine seeps in shallow seas where gas was actually observed (also through hydro-acoustic images)
5 to reach the surface but the output to the atmosphere was not provided, or where, due to the shallow
6 seabed (<400-500 m), the methane is expected to enter the atmosphere. These areas (16 zones) are in the
7 offshore of USA, Canada, Mexico, The Netherlands, Denmark, France, Italy, Greece, Russia, Azerbaijan,
8 Turkmenistan and Pakistan.

9 The dataset does not include deep-sea seeps or areas with gas-charged sediments (e.g. as those
10 inventoried by Fleischer et al. 2001) that may release methane into the water column, but for which the
11 possibility of injection into the atmosphere is scarce or unknown. The area and methane flux estimates
12 reported in the several papers were used here without critical evaluation. Geo-referenced polygons were
13 created for each area (Fig. 5).

14

15

16 **5.2 Attribution of seepage levels**

17 CH₄ fluxes from the original publications (Table S4) are used in the gridded emission dataset.

18

19

20 **5.3 Attribution of the $\delta^{13}\text{C}$ value**

21 The $\delta^{13}\text{C}$ -CH₄ values of SS are attributed on the basis of available literature or considering the geological
22 setting (type of petroleum system, origin of the gas) of the seepage areas (*italic* values in Table S4)
23 following the same criteria adopted for OS. For four areas in Table S4 (China-Brunei offshore, Laurentian
24 Channel and Grand Banks Downing Basin in Canada, and East Kamtchatka shelf in Russia) it was not
25 possible to attribute any theoretical $\delta^{13}\text{C}$ value because the gas may actually derive from either microbial or
26 thermogenic sources, covering a wide range of isotopic values. In these cases, the global emission-
27 weighted $\delta^{13}\text{C}$ value of SS (see Section 5.5.1) was used for these regions in the $\delta^{13}\text{C}$ grids. The global map
28 of $\delta^{13}\text{C}$ for SS is shown in Fig. S5 in the Supplement.

29

30

31 **5.4 SS gridding**

32 The SS grid dataset was generated digitizing polygons of the SS areas from literature maps (see references
33 in Table S4). The final shapefile contains 31 polygons characterized by the following variables: country,
34 longitude and latitude of the polygon centroid, CH₄ output flux, area, and average $\delta^{13}\text{C}$ value of the
35 emissions in each polygon. The value -9999 is reported for the missing emissions at 16 sites (sites 16 to 31
36 in Table S4). The SS layer was joined with the 1°x1° vector grid and the resulting map is shown in Fig. 6.

37

38



1 **5.5 Evaluation of global SS emission and $\delta^{13}\text{C-CH}_4$**

2 The sum of CH_4 emissions from the 15 SS areas in Table S4 (which refer to published estimates) is $3.92 \text{ Tg year}^{-1}$. This represents about 20% of the theoretical estimate of global SS emission to the atmosphere (~ 20
3 Tg year^{-1}), derived by process-based models, proposed by Kvenvolden et al (2001). SS emissions also
4 occur in the other 16 areas reported in Table S4 and likely in many other sites not investigated yet. Among
5 the areas with missing emission values, the Gulf of Mexico and the Caspian Sea are very likely major
6 methane emitters, followed by the North US Atlantic margin. It is difficult to evaluate whether adding these
7 missing SS emissions, the total sum would approach the global theoretical of 20 Tg year^{-1} . Evaluation of the
8 SS emission factor (based on the reported area and total fluxes in Table S4) is also difficult because the
9 areas indicated in the several works (see References in Table S4) often refer to the surveyed area and not
10 to the actual area of seepage; in these cases, using the surveyed area would result in a strongly
11 underestimated emission factor. However, using the relationship observed for the 15 “investigated” sites
12 between area (actual seepage or surveyed) and emission factor, the other 16 sites would yield total
13 emissions of about 1 Tg year^{-1} . This would bring the total CH_4 emission from the 15+16 sites of Table S4 to
14 about 5 Tg year^{-1} . Assuming that (a) SS generally do not take into account the release of dissolved methane
15 (i.e., only methane bubbles are accounted for) and (b) today unknown SS areas (not listed in Table S4) may
16 have a seepage extent not exceeding that of the investigated areas, it is plausible to consider that global SS
17 emission may range between 5 and 10 Tg year^{-1} . If the upper estimate for the East Siberian Arctic Shelf, 4
18 Tg year^{-1} (Berchet et al., 2016; i.e., twice the mean used in Table S4), is considered, then the global SS
19 emission would be between 7 and 12 Tg year^{-1} . The SS emission-weighted mean value of $\delta^{13}\text{C-CH}_4$ is -
20 59‰. The non-weighted mean value is -51.2‰.

22

23

24 **5.6 SS uncertainties**

25 *Spatial distribution uncertainty:* In the $1^\circ \times 1^\circ$ grid, the uncertainty of the geographic distribution of the SS is
26 practically zero, as all seepage zones have geographic coordinates within an error $< 1^\circ$.

27 *Emission uncertainty:* The main uncertainty and control on the global gridded 3.9 Tg year^{-1} value is
28 associated with the estimate of CH_4 emissions from the East Siberian Arctic Shelf, for which we used the
29 central value (2 Tg year^{-1}) of the range indicated by Berchet et al (2016), i.e. $0\text{-}4 \text{ Tg year}^{-1}$. The other 15 SS
30 areas, totaling $\sim 1 \text{ Tg year}^{-1}$, have variable uncertainty, often not defined in the individual publications.

31 *$\delta^{13}\text{C-CH}_4$ uncertainty:* The maximum uncertainty of the estimated $\delta^{13}\text{C}$ values (based on criteria described in
32 Section 5.3) is approximately within $\pm 15\%$, i.e. half of the range of $\delta^{13}\text{C}$ values for typical microbial (-80 to -
33 60%) and thermogenic (-50 to -20%) gas. The uncertainty of the emission-weighted mean (-59%) is mainly
34 controlled by emissions from Eastern Siberian Arctic Shelf, North Sea and Black Sea, whose $\delta^{13}\text{C}$ values are
35 available or estimated, ranging from -50 to -63% . The overall uncertainty of the global emission-weighted
36 mean is thus reasonably $< \pm 7\%$.

37

38



1 **6 Microseepage (MS)**

2

3 **6.1 Assessment of global MS area**

4 The diffuse exhalation of CH₄, called microseepage (MS), is widespread throughout petroleum fields all over
5 the world. It is systematically observed in correspondence with anticlines and marginal (faulted) areas of
6 gas-oil fields (Etiopie and Klusman, 2010; Tang et al. 2017). The existence of macro-seeps (OS) in a given
7 region also implies a high probability that MS exists in that region, even if that region falls outside a known
8 petroleum field. Therefore, as a proxy of the activity (spatial distribution) of MS, we considered the global
9 area of petroleum fields and a global area including OS defined as described below. This criterion is
10 conservative as MS may also occur in sedimentary basins without known petroleum fields and OS (Klusman
11 et al. 2008; Etiopie and Klusman, 2010). The assessment of the global petroleum field area (PFA) and global
12 OS area (OSA) is discussed in the Supplement (Sections S3.1 and S3.2). The total potential MS area (PMA)
13 resulted to be PFA + OSA = 13,033,000 + 85,900 = 13,118,900 km².

14

15

16 **6.2 Attribution of MS levels**

17 The level of MS CH₄ emissions was established on the basis of a statistical analysis of a MS flux data-set
18 (see Section 6.2.1) and considering the theory of seepage migration mechanisms, for which the gas flux
19 greatly depends on the permeability of the rocks, especially when induced by faults and fracture networks
20 (Etiopie and Klusman, 2010; Etiopie, 2015; Tang et al. 2017). Accordingly, the attribution of the flux within the
21 PMA (PFA+OSA) was done considering the presence/absence, in each cell, of three major geological
22 factors, which are proxies of methane seepage and gas permeability, i.e. OS, faults and seismicity, as
23 explained in Section 6.2.2.

24

25 **6.2.1 Statistics of MS data**

26 A dataset of 1509 MS CH₄ flux measurements was compiled based on available literature and unpublished
27 works. The data are from 19 petroleum areas: 8 in the USA (Klusman et al 2000; Klusman, 2003; Klusman,
28 2005; Klusman, unpublished; LTE, 2007), 6 in Italy (Etiopie and Klusman, 2010; Sciarra et al. 2013; Etiopie,
29 2005; Etiopie, unpublished), 1 in Romania (Etiopie, 2005), 1 in Greece (Etiopie et al. 2006; Etiopie,
30 unpublished), and 3 in China (Tang et al. 2007; 2010; 2017). The resulting descriptive statistics are reported
31 in Table S5 in the Supplement.

32 The data are divided into two groups: (a) negative and near-zero values (<0.01 mg m⁻² d⁻¹, considering
33 minimum analytical error), which represent the normal CH₄ flux in dry (not flooded) soils, and (b) positive
34 values, >0.01 mg m⁻² d⁻¹ (i.e. microseepage). The similar order of magnitude between the median and the
35 geometric mean flux indicates a log-normal behavior of the positive CH₄ flux distribution. The positive values
36 represent about 57% of total measurements. This implies that MS does not occur throughout the entire PFA.
37 This is well known, as CH₄ flux from the ground, in addition to underground rock permeability and fluid
38 pressures, depends also on soil conditions (humidity, porosity, temperature) and methanotrophic activity.



1 Accordingly, and taking into account that the MS measured sites are geographically dispersed with a
2 relatively homogeneous spatial distribution (and the measurements were taken in different seasons), we
3 reduced the PFA by removing 43% of the area as described in Section 6.4. A new MS area was therefore
4 defined as “Effective Microseepage Area”, EMA, which is OSA + 57% of PFA. The derivation of the EMA
5 area is described in Section 6.4. Frequency histogram and Normal Probability Plot (NPP) of MS data
6 (logarithmic values of positive values) confirm that flux values have a log-normal distribution (Fig. S7).
7 Values exceeding $1000 \text{ mg m}^{-2} \text{ d}^{-1}$ (up to 7078) were excluded as they represent special and rare cases of
8 MS (often not distinguishable from miniseepage, which is the halo surrounding macro-seeps).

9 The combined analysis of NPP and frequency histogram (Fig. S7) resulted in the identification of 4 main
10 groups of positive flux data, i.e. 4 levels of MS:

11 Level 1 0.01-12 (median: 1.3) $\text{mg m}^{-2} \text{ d}^{-1}$

12 Level 2 12-60 (median: 31.1)

13 Level 3 60-300 (median: 110)

14 Level 4 300-1000 (median: 493.5)

15 Level 0 implies absence of MS. The median of each level was assigned to the $0.05^\circ \times 0.05^\circ$ grid cells
16 included in the area with expected MS defined in Section 6.2.2 and according to the presence of the factors
17 influencing MS. The median was chosen because it is not affected by outliers within each level, providing
18 conservative flux values.

19

20

21 *6.2.2 Factors influencing MS level: presence of macro-seeps, faults and seismicity.*

22 The 4 MS levels (1, 2, 3 and 4) are associated with 4 different combinations of the three factors influencing
23 the gas flux, following MS theory and experimental data. The three factors are:

24 (a) faults;

25 (b) seismic activity;

26 (c) presence of macro-seeps (OS), which are themselves expression of regional seepage activity;

27

28 (a) Fault data were taken from 17 different datasets (see Sources of databases in the Supplement): the main
29 one is the Global Faults layer of ArcAtlas (Finko, 2014). It includes two types of faults: (1) faults created by
30 the dislocation of rocks that define the geological structures of the continents (tectonic contacts and thrust-
31 faults) and (2) faults created by the morphology of the present-day relief and morphostructure (steps and
32 rifts). The first type of faults refers to ancient structures, while those revealed by relief are comparatively
33 young structures that appeared during the neotectonic stage of the Earth's evolution (mostly in the Neogene
34 and Quaternary periods). The other 16 fault datasets are national or regional datasets from Afghanistan,
35 Australia, Bangladesh, Caribbean region, Central Asia, Europe including Turkey, Georgia, Greece, Ireland,
36 Italy, New Zealand, South America, Southern Mediterranean area, Spain, Switzerland, United Kingdom (see
37 Supplement). The final merged fault dataset includes 156,095 tectonic elements (Fig. S8); obviously it does
38 not include all actual existing faults on Earth. The dataset must be interpreted as a global distribution of the
39 main regional fault systems and fractured zones.



1

2 (b) The epicenters of earthquakes are proxies of fault location and activity (permeability), so they also
3 represent the presence of active faults, which may not be reported in the fault dataset. It is also known that
4 gas migration and escape to the surface may increase with seismic activity. We used the seismicity dataset
5 of USGS Earthquake Lists, Maps and Statistics (see Sources of databases in the Supplement). We
6 extracted only onshore seismic events with magnitude $M > 4.5$ recorded from 2005 to 2017. This resulted in a
7 dataset of 18,157 onshore epicenters covering 177 countries (Fig. S9).

8

9 (c) Presence of macro-seeps (OS). The OS area is described in the Supplement (Section S3.2).

10

11 The three factors, faults, seismicity and presence of seeps, were applied on the gridded EMA as described
12 in Section 6.4.

13

14

15 **6.3 Attribution of the $\delta^{13}\text{C}$ value**

16 Measured and published data of $\delta^{13}\text{C}\text{-CH}_4$ in gas MS are scarce and available only for a few petroleum
17 fields. However, during the seepage process (migration driven by pressure gradients, i.e. advection), the
18 CH_4 isotopic composition does not change significantly, so that surface CH_4 flux has basically the same $\delta^{13}\text{C}$
19 value of the original gas in the reservoir (e.g., Etiope et al. 2009). Therefore, for each field or basin, the MS
20 $\delta^{13}\text{C}$ value was taken from published data related to subsurface reservoirs. A limitation of this strategy is that
21 in a given basin the MS gas may come from shallower reservoirs, not necessarily or not dominantly from the
22 deep productive reservoirs, which are more frequently the literature source of the isotopic value. Therefore,
23 in some cells the actual isotopic value could be lighter than in the grid maps.

24 Accordingly we adopted the following procedure:

25 - when one or more seeps (OS) occur in a petroleum field (in the Petrodata list), the average $\delta^{13}\text{C}\text{-CH}_4$ of
26 those seeps was used for MS;

27 - in absence of seeps, reservoir $\delta^{13}\text{C}\text{-CH}_4$ data were used; they were taken from the inventory described by
28 Sherwood et al. (2017) or published literature. For the fields (in the Petrodata list) whose $\delta^{13}\text{C}\text{-CH}_4$ value is
29 not reported either in Sherwood et al. (2017) or literature, a theoretical $\delta^{13}\text{C}\text{-CH}_4$ value was estimated on the
30 basis of the type of gas (microbial or thermogenic) and maturity of the petroleum system.

31 The file contains 349 $\delta^{13}\text{C}\text{-CH}_4$ data points (from 891 petroleum fields). It was not possible to estimate a
32 specific $\delta^{13}\text{C}$ value for the remaining 542 petroleum fields. In these cases, the global emission-weighted
33 isotopic value was used in the resulting empty cells, as described in Section 6.4.

34

35

36 **6.4 MS gridding**

37 PFA and OSA (described in the Supplement) were intersected with a high-resolution ($0.05^\circ \times 0.05^\circ$) global
38 grid. The $0.05^\circ \times 0.05^\circ$ cell dimension corresponds to the maximum resolution that can be obtained using



1 ArcGIS software (the software cannot handle shapefiles > 2 Gbyte). The high-resolution gridding was used
2 to match, as much as possible, the PFA: gridded PFA is in fact 14,791,897 km², while the original PFA was
3 13,033,750 km². The high-resolution gridding also served to reduce the boundary effect, and thus the
4 overestimation of the areas with MS enhancing factors, i.e. faults, earthquake and seeps (the larger the
5 cells, the higher the probability that the cells include MS enhancing factors).

6 As discussed in Section 6.2.1, only 57% of PFA cells were considered to host MS. It was then necessary to
7 delete 43% of PFA cells. The cells were randomly deleted only among those that do not host MS enhancing
8 factors (faults, earthquakes and seeps), i.e. empty cells (which are 93% of total PFA). The overall PFA
9 reduction of 43% was obtained by deleting 54% of the empty cells (resulting in a PFA of 8,408,360 km²).
10 Combining PFA and OSA results in EMA (Table S6). The sequence of MS modeling is summarized in the
11 block diagram of Fig. S10. The MS levels were then assigned to the 0.05°x0.05° gridded EMA according to
12 the presence of the factors influencing MS: a) presence of faults; b) presence of seismic activity; c) presence
13 of macro-seeps (OS), as follows:

14 Level 1 was applied to cells without any geological factor.

15 Level 2 was applied to cells with faults or earthquakes

16 Level 3 was applied to cells with faults plus earthquakes or oil-seeps or gas-bearing springs

17 Level 4 is applied to cells with gas-seeps or mud volcanoes.

18 The resulting global MS CH₄ emissions are about 24 Tg/y. The emissions per cell range from 14.7 tonnes
19 year⁻¹ (cells of about 30 km²) to 29,446 tonnes year⁻¹ (cells of about 169 km²). The grid was then converted
20 into 1°x1° resolution for atmospheric modelling applications (Fig. 7). MS emissions occur in 3,039 cells,
21 ranging from 15 to 471,000 tonnes year⁻¹. The cell with the highest emission is located in the Caspian region
22 (Azerbaijan). The sensitivity of the MS modeling is discussed in the Supplement (Section S3.3).

23

24

25 **6.5 Evaluation of global MS emission and $\delta^{13}\text{C-CH}_4$**

26 The global MS emission derivable by summing the emission from the cells of the 4 MS classes, about 24 Tg
27 year⁻¹ (Table S6), is within the range, 10-25 Tg year⁻¹, previously suggested by Etiope and Klusman (2010).

28 The emission-weighted $\delta^{13}\text{C-CH}_4$ resulting from gridded MS is -51.4‰ (non-weighted average is -46.4‰).
29 This value is mostly influenced by areas with elevated MS of microbial gas, such as the Po Basin (Italy), the
30 Transylvania Basin (Romania) and the Powder River Basin (USA). The global emission-weighted value was
31 applied to cells without isotopic value.

32

33

34 **6.6 MS uncertainties**

35 *Spatial distribution uncertainty:* The uncertainty of the spatial distribution of MS depends on the assumption,
36 supported by field measurements, that MS occurs significantly only within petroleum fields (PFA) and areas
37 with seeps (OSA). The uncertainty of PFA depends on the "Petrodata" dataset of Päivi et al. (2007),
38 discussed in section 5.1, and it cannot be quantified. The uncertainty of OSA depends on the buffer applied
39 to individual seeps, which was however defined by geospatial analysis (Section 6.1.2).



1 *Emission uncertainty*: The uncertainty of the MS emission depends on the activity (EMA) and on the
2 process-based model of attribution of the seepage levels (emission factors), and their statistical elaboration,
3 discussed in section 6.2 (see also Fig. S10). Changing activity by $\pm 20\%$ and emission factor by the 95%
4 confidence interval of the median, with different combinations, resulted in a total MS output ranging from 15
5 to 32.7 Tg year⁻¹, with a mean of 23 Tg year⁻¹, matching the first estimate (see Supplement). We can
6 therefore set, approximately, a maximum uncertainty in the total MS output of ± 9 Tg year⁻¹ (about $\pm 38\%$).

7 The model was then tested comparing its output values with measured values. This comparison was
8 possible for 9 areas where the coordinates of the measurement points were identified. In all cases,
9 measured and modeled values have the same order of magnitude, and in many cases the range of the MS
10 level attributed by the model includes the mean value measured.

11 *$\delta^{13}\text{C}$ uncertainty*: The uncertainty of individual MS $\delta^{13}\text{C}$ values depends on the assumptions discussed in
12 Section 6.3. The uncertainty of the emission-weighted mean (-51.4‰) is mainly controlled by the cells with
13 larger MS emissions where $\delta^{13}\text{C}$ values are estimated. When the cells with emission-weighted mean are
14 excluded, the remaining 536 cells (at $0.05^\circ \times 0.05^\circ$, over a total of 192,166) have emission ranging from 5623
15 to 8296 tonnes year⁻¹ and $\delta^{13}\text{C}$ values from -65 to -35‰ (mean -53.4‰). The difference of this value with the
16 emission-weighted mean, i.e., 2‰ , may be considered as approximate expression of the uncertainty of the
17 global emission-weighted mean.

18

19

20 **7. Geothermal manifestations (GM)**

21

22 **7.1 Global GM distribution**

23 The global distribution of CH₄-emitting geothermal/volcanic sites (GM) generated here is based on an
24 inventory of volcanoes and geothermal sites developed by Global Volcanism Program (2013) (see Sources
25 of databases in the Supplement). This inventory reports all major volcanic-geothermal systems on Earth
26 (2,378 sites; Fig. S12). They include both Holocene systems (1,307 sites distributed in 128 countries), and
27 older, Pleistocene volcanic systems (1,071 sites distributed in 119 countries), which represent geothermal
28 areas. In order to convert the point data into more realistic areal data (polygons), a buffer area of 4 km of
29 radius was created for each GM point (the choice of 4 km is based on approximate average evaluations of
30 GM areal extensions derived from Google Earth and published material). It is important to outline that this
31 inventory reports the “zones” of volcanic/geothermal sites, and does not list individual manifestations: for
32 example, the numerous geothermal manifestations in Central Italy are cumulatively included in a few lines,
33 e.g., “Vulsini complex”, “Sabatini complex” and “Vulture”.

34

35

36 **7.2 Attribution of CH₄ emission levels**

37 Methane flux measurements and regional total estimates in GM are available only in a few cases, mostly in
38 Europe (as reviewed by Etiope et al. 2007). The GM inventory refers to geothermal-volcanic areas where



1 GMs are expected to occur, but their actual surface area is unknown. Therefore, even assuming an
2 emission factor (from the limited flux dataset) it cannot be translated into emission for each GM site. In this
3 work, theoretical “working numbers” were adopted considering 3 classes of emissions: 500, 5000, 10000
4 tonnes year⁻¹, as representative of the “probable” order of magnitude (e.g., 500 means an order of
5 magnitude of 10² tonnes year⁻¹) derived from the typical CH₄ fluxes in geothermal areas, measured mainly in
6 Europe (Etiope et al. 2007 and Refs. therein). Accordingly, the total emission estimate suggested by the
7 emission grid is not meant to update or refine the previous global GM emission estimate (Etiope et al. 2008).
8 The emission level was attributed based on:

9 (a) the location of the geothermal site, which may be within or outside a sedimentary basin (Fig. S13),

10 (b) the concentration of CH₄ measured in the geothermal fluids, within and outside a sedimentary basin.

11 The amount of methane in a geothermal-volcano area depends, in fact, on the presence of sediments rich in
12 organic matter, which may be source of thermogenic gas in addition to the geothermal abiotic gas. The
13 CO₂/CH₄ ratio of emissions to the atmosphere is in the order of 1000-10,000 in volcanic sites, with limited
14 sedimentary contribution, and it ranges from 1 to 100 in geothermal systems characterized by important
15 sedimentary covers. Sediment-Hosted Geothermal Systems (SHGS) in sedimentary basins (e.g., Etiope,
16 2015; Procesi et al, submitted) show the highest CH₄ concentrations (lowest CO₂/CH₄ ratio). In addition,
17 sedimentary basins hosting petroleum fields reasonably contain larger amounts of methane. The three
18 classes of methane emissions are defined as explained in Section 7.4.

19

20

21 **7.3 Attribution of the $\delta^{13}\text{C}$ value**

22 A specific dataset was compiled listing 98 published $\delta^{13}\text{C}$ -CH₄ values of various, geographically dispersed,
23 geothermal/volcanic systems in the world. The isotopic $\delta^{13}\text{C}$ -CH₄ values range from -43.2 to -6.4‰, with an
24 average of -26.7‰. The double-sided Grubs test identified 4 outliers; the mean $\delta^{13}\text{C}$ -CH₄ value of the 94
25 values excluding the outliers is -26.5‰. It is known that geothermal methane in sedimentary basins has a
26 lower $\delta^{13}\text{C}$ -CH₄ value compared to sediment-free systems. The NPP of the $\delta^{13}\text{C}$ -CH₄ data shows a sharp
27 deviation at about -29‰ (Fig. S14). This value is actually consistent with the isotopic boundary of dominantly
28 thermogenic gas; we used therefore this value as limit between GM falling outside sedimentary basins and
29 GM within sedimentary basins. The mean values of the two classes (excluding the outliers) are summarized
30 in Table S8.

31

32

33 **7.4 GM gridding**

34 The GM shapefile generated in ArcGIS environment was spatially joined to the 1°x1° vector square grid. The
35 result is reported in Table S9 and mapped in Fig. 8.

36

37

38



1 **7.5 Evaluation of global GM emission and $\delta^{13}\text{C-CH}_4$**

2 The 2,378 GM sites yield total methane emission of about 5.7 Tg year^{-1} , which is within the range of the
3 latest global GS emission estimate ($2.2\text{-}7.3 \text{ Tg year}^{-1}$; Etiope, 2015). The emission-weighted mean value of
4 $\delta^{13}\text{C-CH}_4$ for the GM emission is -30.6‰ (non-weighted mean is -27.5‰).

7 **7.6 GM uncertainties**

8 *Spatial distribution uncertainty:* The uncertainty of the spatial distribution of GM has the same uncertainty as
9 the global distribution of geothermal-volcanic areas, derived from Global Volcanism Program (2013)..

10 *Emission uncertainty:* Emission values attributed to GM are theoretical estimates, consistent however with
11 the emission factor dataset and with the global GM emission, published in the literature, derived from
12 process-based models.

13 *$\delta^{13}\text{C}$ uncertainty:* The uncertainty of emission-weighted GM $\delta^{13}\text{C}$ may refer to the average of the two values
14 corresponding to the 95% confidence interval of the means of the two groups of isotopic data (outside and
15 within sedimentary basins) discussed in section 6.3, i.e. $\pm 2.5\text{‰}$.

19 **8. Merging OS, SS, MS and GM: total geo- CH_4 emission gridding**

21 **8.1 Global geo- CH_4 emission**

22 The global geo- CH_4 emission distribution, obtained merging OS, SS, MS and GM grids, is shown in Fig. 9.
23 The total gridded CH_4 emission is 37.4 Tg/y (Table 3, second column). The extrapolated gridded emission
24 estimate including the factors not considered in the gridding procedure (i.e. mud volcano eruptions,
25 existence of onshore and offshore seeps not included in the OS-SS inventories) is between about 43 and 50
26 Tg year^{-1} (Table 3, third column). These values are within the published global bottom-up estimates (Table
27 3, fourth column). The global extrapolated geo- CH_4 emission is then compatible with recent top-down
28 estimates (about 50 Tg year^{-1} by Schwietzke et al. 2016).

29 Considering the four geo- CH_4 source categories individually, the gridded MS and GM emission totals are
30 within published ranges. The differences between gridded and published OS and SS are largely due to:

- 31 - incomplete OS dataset (it represents only 30% of global number of seeps assumed to exist on Earth)
- 32 - lower estimate of the global MV area (680 km^2 instead of 2800 km^2 assumed in previous works)
- 33 - incomplete SS flux dataset (flux data missing from at least 16 areas with known gas emissions).

34 The gridded emissions may represent an updated assessment of the global emissions only for MS and MVs
35 (part of OS).

36
37
38
39



1 **8.2 Global geo-CH₄ δ¹³C**

2 Based on the emission-weighted δ¹³C value for each category of emission (using the respective emissions
3 from Table 3), the global geo-CH₄ emission-weighted average δ¹³C is -49.4‰, considering global emission
4 estimates and -48.5‰ for gridded emissions (Table 4). The global distribution of the isotopic signature is
5 shown in Fig. 10.

6
7

8 **8.3 Uncertainties of gridded geo-CH₄ distribution, emission and isotopic value**

9 The overall uncertainties of the spatial distribution of the geo-CH₄ sources, CH₄ emissions and emission-
10 weighted average values of δ¹³C, depend on individual uncertainties of the four categories of seepage, as
11 discussed in the respective Sections 4.6, 5.6, 6.6 and 7.6. These are summarized in Table 5.

12

13

14 **9. Summary and Conclusions**

15 Gridded maps of global geological CH₄ emissions at 1°x1° resolution have been developed comprehensively
16 for the first time for atmospheric modeling and evaluation of global CH₄ sources. The maps, elaborated by
17 ArcGIS and provided as csv files, include the four main categories of natural geological CH₄ emissions:
18 onshore hydrocarbon seeps (OS), submarine (offshore) seepage (SS), diffuse microseepage (MS), and
19 geothermal manifestations (GM). A combination of published and originally *ad-hoc* developed datasets was
20 used to determine the emission factors and the areal distribution and extent (activity) of the several geo-CH₄
21 sources and their stable carbon isotope signature (δ¹³C). Due to the limited number of direct CH₄ flux
22 measurements, globally and regionally representative CH₄ emission factors for OS, MS and GM were
23 estimated based on experimental emission factors (measurements) and statistical approaches. Methane
24 emission estimates for SS were adopted directly from published regional emission estimates. The results of
25 this work can be summarized as follows:

26

27 (a) The global geo-CH₄ source map reveals that the regions with the highest CH₄ emissions are all located
28 in the northern hemisphere, in North America, in the Caspian region, Europe, and in the East Siberian Arctic
29 Shelf.

30 (b) The globally gridded CH₄ emission estimate (37 Tg year⁻¹ exclusively based on data and modeling
31 specifically targeted for gridding, and 43-50 Tg year⁻¹ when extrapolated to also account for onshore and
32 submarine seeps with no location specific measurements available) is compatible with published ranges
33 derived by top-down and bottom-up procedures.

34 (c) The procedures adopted to attribute CH₄ fluxes to mud volcanoes (MV, a OS sub-class) and
35 microseepage (MS) are based on a detailed assessment of the activity (areas) and emission factors, and the
36 resulting gridded total output can be considered a refinement of previously published emission estimates.
37 Specifically, the global MV emission estimate (2.8 Tg year⁻¹, excluding eruptions) is compatible with early
38 estimates by Dimitrov (2002), Milkov et al (2003), Etiope and Milkov (2004) and Etiope et al (2008). Global



1 MS emissions (previously estimated between 10 and 25 Tg year⁻¹; Etiope and Klusman, 2010) are now
2 estimated to be ~24 (±9) Tg year⁻¹.

3

4 (d) Regional emissions of SS are available from the literature for only a limited number of cases. The
5 regions with missing emission data in the literature are not included in the gridded dataset developed here.
6 As a result, the gridded CH₄ emission estimate (3.9 Tg year⁻¹) is substantially smaller than a previously
7 published global total estimate (20 Tg year⁻¹, which would include extrapolated values to regions without
8 region-specific estimates (Kvenvolden et al. 2001). However, the published SS estimate has large
9 uncertainties (at least 10 Tg CH₄ year⁻¹ since two separate estimates of 10 and 30 Tg CH₄ year⁻¹ were
10 actually provided without indication of their uncertainties) and it was purely based on process-based
11 modelling (Kvenvolden et al. 2001). This work verified that SS emissions also occur in other regions where
12 emission values are missing (among these, the Gulf of Mexico, Caspian Sea and the North US Atlantic
13 margin). Given an estimated SS emission factor, we propose that global SS CH₄ emissions may range
14 between 5–12 Tg year⁻¹, with a best guess (central value) of 8.5 Tg year⁻¹.

15

16 (e) The emission-weighted global mean of δ¹³C-CH₄ is -48.5‰ for the gridded emissions, and -49.4‰ when
17 gridded OS and SS emissions are extrapolated to include all global regions. These values are significantly
18 lower (about 4-5‰ lighter) than typical values attributed to fossil fuel industry sources (-44‰ by Schwietzke
19 et al, 2016) and much lower (10-11‰ lighter) than seepage values considered in inverse studies (-38‰ by
20 Sapart et al. 2012). Clearly, natural geological sources are more ¹³C-depleted than generally assumed (and
21 this mostly occurs as microseepage and submarine seepage). Low maturity thermogenic gas and microbial
22 gas are, in fact, a neglected, but considerable, fraction of the global fossil CH₄ budget (Sherwood et al.
23 2017). It is expected that using the updated, more ¹³C-depleted, isotopic signatures in atmospheric
24 modelling studies will increase the top-down estimate of the global geological CH₄ sources (all else equal).

25

26 The maps developed here represent important inputs for future atmospheric modeling of the global CH₄
27 cycle. Fossil fuel industry “upstream” activities (exploration, production, and some processing of fossil fuels)
28 and associated CH₄ emissions occur largely on land surface above sedimentary basins that are also the
29 habitat for geological CH₄ seepage. Thus, there is substantial spatial overlap in CH₄ emissions from the
30 fossil fuel industry and geological seepage. Nevertheless, there is substantial spatial variability in CH₄
31 emission intensity for both the fossil fuel industry (Maasackers et al. 2016; JBC/PBL, 2017) and geological
32 seepage (this work). In the absence of a comprehensive gridded geological CH₄ seepage product, global or
33 regional inverse model studies would erroneously attribute a low-bias to CH₄ emissions from geological
34 seepage and a high-bias to CH₄ emissions from fossil fuel industry activity. The geological seepage data
35 and maps developed here can be used to refine fossil fuel industry and microbial CH₄ emission budgets at
36 the regional and global level. Finally, methane/ethane and methane/propane source composition ratios are
37 available for the four categories of geo-sources (preliminary data were used in Etiope and Ciccioli, 2009) for
38 use beyond the scope of this work. Combining the gridded geo-CH₄ emissions and the available source
39 composition data, gridded ethane and propane maps could be developed in the future. The gridded geo-CH₄



1 maps shall be updated when additional, statistically significant gas flux data for the several seepage
2 categories become available. Geo-CH₄ emission from a fifth, recently discovered, geological category, the
3 seepage from serpentinized peridotites (e.g., Etiope et al. 2017 and references therein) shall also be gridded
4 when sufficient flux data become available.

5

6

7 **10 Data availability**

8

9 The free availability of the data does not constitute permission for their publication. If the data are essential
10 to new modelling, or to develop results and conclusions of a paper, co-authorship may need to be
11 considered. Grid csv files (emission and isotopic composition for each geological source and integrated grid
12 files) and microseepage and geothermal manifestations inventories are available at
13 <https://doi.org/10.25925/4j3f-he27> (Etiope et al. 2018), including full contact details and information on how
14 to cite the data. The SS inventory is provided in the Supplement (Table S4). Due to CGG (2015) license
15 restrictions, the OS inventory can be requested at

16 www.cgg.com/en/What-We-Do/Multi-Client-Data/Geological/Robertson-Geochemistry.

17 The datasets of petroleum fields, faults, volcanic-geothermal sites, earthquakes, sedimentary basins are
18 available on the web as described in the Supplement.

19

20 The Supplement related to this article is available online at

21

22 Competing interests. The authors declare that they have no conflict of interest.

23

24 **Acknowledgements.** The work was supported by NASA grant NNX17AK20G. Thanks are due to Lori Bruhwiler for
25 revising the manuscript.

26

27

28 **References**

29

30 Aliyev, A. A., Guliyev, I. S., and Feyzullayev, A. A.: What do we know about mud volcanoes Azerbaijan National
31 Academy of Sciences Geology Institute, Qoliaf qrup QSC, Baku, 206 pp., 2012.

32

33 Berchet, A., Bousquet, P., Pison, I., Locatelli, R., Chevallier, F., Paris, J.-D., Dlugokencky, E. J., Laurila, T., Hatakka, J.,
34 Viisanen, Y., Worthy, D. E. J., Nisbet, E., Fisher, R., France, J., Lowry, D., Ivakhov, V., and Hermansen, O.: Atmospheric
35 constraints on the methane emissions from the East Siberian Shelf, *Atmos. Chem. Phys.*, 16, 4147–4157, 2016.

36

37 Bergamaschi, P., Houweling, S., Segers, A., Krol, M., Frankenberg, C., Scheepmaker, R. A., Dlugokencky, E., Wofsy, S.
38 C., Kort, E. A., Sweeney, C., Schuck, T., Brenninkmeijer, C., Chen, H., Beck, V., and Gerbig, C.: Atmospheric CH₄ in the
39 first decade of the 21st century: Inverse modeling analysis using SCIAMACHY satellite retrievals and NOAA surface
40 measurements, *J. Geophys. Res.-Atmos.*, 118, 7350–7369, doi:10.1002/jgrd.50480, 2013.

41

42 Bousquet, P., Ciais, P., Miller, J. B., Dlugokencky, E. J., Hauglustaine, D. A., Prigent, C., Van der Werf, G. R., Peylin, P.,
43 Brunke, E. G., Carouge, C., Langenfelds, R. L., Lathiere, J., Papa, F., Ramonet, M., Schmidt, M., Steele, L. P., Tyler, S.
44 C., and White, J.: Contribution of anthropogenic and natural sources to atmospheric methane variability, *Nature*, 443,
45 439–443, 2006.

46

47 CGG: Organic Geochemistry Data from FRogi and Fluid Features Database, www.cgg.com/en/What-We-Do/Multi-Client-Data/Geological/Robertson-Geochemistry, 2015.

48

49 Ciais, P., Sabine, C., Bala, G., Bopp, L., Brovkin, V., Canadell, J., Chhabra, A., DeFries, R., Galloway, J., M., H., Jones,
50



- 1 C., Le Quéré, C., Myneni, R. B., Piao, S., and Thornton, P.: Carbon and Other Biogeochemical Cycles, in: Climate
2 Change 2013: The Physical Science Basis. Contribution of Working Group I to the Fifth Assessment Report of IPCC,
3 edited by: Stocker, T. F., Qin, D., Plattner, G.-K., Tignor, M., Allen, S. K., Boschung, J., Nauels, A., Xia, Y., Bex, V., and
4 Midgley, P. M., Cambridge University Press, Cambridge, UK, 2013.
5
- 6 Clarke, R. H., and Cleverly R. W.: Leakage and post-accumulation migration, In: England WA, Fleet AJ (eds) Petroleum
7 migration, vol 59, Geological Society Special Publication, London, pp 265–271, 1991.
8
- 9 Dimitrov, L.: Mud volcanoes - the most important pathway for degassing deeply buried sediments, *Earth-Sci. Rev.*, 59,
10 49–76, 2002.
11
- 12 Dimitrov, L.: Mud volcanoes - a significant source of atmospheric methane, *Geo-Mar. Lett.*, doi: 10.1007/s00367–003–
13 0140–3, 2003.
14
- 15 Etiope, G.: Mud volcanoes and microseepage: the forgotten geophysical components of atmospheric methane budget.
16 *Annals of Geophysics*, 48, 1-7, 2005.
17
- 18 Etiope, G.: Methane uncovered. *Nature Geosci.*, 5, 373-374, 2012.
19
- 20 Etiope, G.: Natural Gas Seepage. *The Earth's hydrocarbon degassing*, Springer, pp. 199, 2015.
21
- 22 Etiope, G.: Natural Gas, *Encyclopedia of Geochemistry*, Earth Sciences Series, Springer, pp.1-5, 2017.
23
- 24 Etiope, G., Baciu, C., Caracausi, A., Italiano, F., and Cosma, C.: Gas flux to the atmosphere from mud volcanoes in
25 eastern Romania, *Terra Nova*, 16, 179-184, 2004a.
26
- 27 Etiope, G., Christodoulou, D., Kordella, S., Marinaro, G., and Papatheodorou, G.: Offshore and onshore seepage of
28 thermogenic gas at Katakolo Bay (Western Greece), *Chem. Geol.*, 339, 115-126, 2013.
29
- 30 Etiope, G., and Ciccio, P.: Earth's degassing - A missing ethane and propane source, *Science*, 323, 478, 2009.
31
- 32 Etiope, G., Ciotoli, G., Schwietzke, S., and Schoell, M.: Global geological CH₄ emission grid files.
33 <https://doi.org/10.25925/4j3f-he27>, 2018.
34
- 35 Etiope, G., Doeze, L., and Pacheco, C.: Emission of methane and heavier alkanes from the La Brea Tar Pits seepage
36 area, Los Angeles, *J. Geophys. Res.-Atm.*, 122, 12,008-12,019, 2017.
37
- 38 Etiope, G., Feyzullayev, A., Baciu, C. L.: Terrestrial methane seeps and mud volcanoes: a global perspective of gas
39 origin, *Mar. Petrol. Geol.*, 26, 333-344, 2009.
40
- 41 Etiope, G., Feyzullaiev, A., Baciu, C. L., and Milkov, A. V.: Methane emission from mud volcanoes in eastern Azerbaijan,
42 *Geology*, 32, 6, 465-468, 2004b.
43
- 44 Etiope, G., and Klusman, R. W.: Geologic emissions of methane to the atmosphere, *Chemosphere*, 49, 777-789, 2002.
45
- 46 Etiope, G. and Klusman, R. W.: Microseepage in drylands: flux and implications in the global atmospheric source/sink
47 budget of methane, *Global. Planet. Change*, 72, 265-274, 2010.
48
- 49 Etiope, G., Lassey, K. R., Klusman, R. W., and Boschi, E.: Reappraisal of the fossil methane budget and related
50 emission from geologic sources, *Geophys. Res. Lett.*, 35, L09307, <https://doi.org/10.1029/2008GL033623>, 2008.
51
- 52 Etiope, G., and Milkov, A. V.: A new estimate of global methane flux from onshore and shallow submarine mud
53 volcanoes to the atmosphere, *Environ. Geol.*, 46, 997-1002, 2004.
54
- 55 Etiope, G., Nakada, R., Tanaka, K., and Yoshida, N.: Gas seepage from Tokamachi mud volcanoes, onshore Niigata
56 Basin (Japan): origin, post-genetic alterations and CH₄-CO₂ fluxes, *Appl Geochem.*, 26, 348-359, 2011.
57
- 58 Etiope, G., Papatheodorou, G., Christodoulou, D., Ferentinos, G., Sokos, E., and Favali P.: Methane and hydrogen
59 sulfide seepage in the NW Peloponnesus petroliferous basin (Greece): origin and geohazard, *Am. Assoc. Pet. Geol.*
60 *Bull.*, 90, 701-713, 2006.
61
- 62 Etiope, G., Samardžić, N., Grassa, F., Hrvatović, H., Miošić, N., and Skopljak, F.: Methane and hydrogen in
63 hyperalkaline groundwaters of the serpentinized Dinaride ophiolite belt, Bosnia and Herzegovina, *Applied Geochem.*, 84,
64 286-296, 2017.



- 1
2 Etiop, G. and Schoell, M.: Abiotic gas: atypical but not rare, *Elements*, 10, 291–296, 2014.
3
4 Etiop, G. and Sherwood Lollar, B.: Abiotic methane on Earth, *Rev. Geophys.*, 51, 276–299, 2013.
5
6 Finko, E. A.: Global faults layer from ArcAtlas (ESRI), Editor: A.A. Liouty,
7 <http://www.arcgis.com/home/item.html?id=a5496011fa494b99810e4deb5c618ae2#overview>, 2014.
8
9 Fleicher, P., Orsi, T. H., Richardson, M. D., and Anderson, A. L.: Distribution of free gas in marine sediments: a global
10 overview, *Geo-Marine Lett.*, 21, 103–122, 2001.
11
12 JRC/PBL - European Commission, Joint Research Centre (JRC)/Netherlands Environmental Assessment Agency (PBL):
13 Emission Database for Global Atmospheric Research (EDGAR), Release EDGARv4.3, Retrieved from
14 <http://edgar.jrc.ec.europa.eu>, 2017.
15
16 Judd, A. G.: Natural seabed seeps as sources of atmospheric methane, *Environ. Geol.*, 46, 988–996, 2004.
17
18 Judd, A. G., and Hovland, M.: *Seabed Fluid Flow: Impact on Geology, Biology and the Marine Environment*, Cambridge
19 University Press, Cambridge, 2007.
20
21 Kirschke, S., Bousquet, P., Ciais, P., Saunoy, M., Canadell, J. G., Dlugokencky, E. J., Bergamaschi, P., Bergmann, D.,
22 Blake, D. R., Bruhwiler, L., Cameron-Smith, P., Castaldi, S., Chevallier, F., Feng, L., Fraser, A., Heimann, M., Hodson,
23 E. L., Houweling, S., Josse, B., Fraser, P. J., Krummel, P. B., Lamarque, J. F., Langenfelds, R. L., Le Quere, C., Naik,
24 V., O'Doherty, S., Palmer, P. I., Pison, I., Plummer, D., Poulter, B., Prinn, R. G., Rigby, M., Ringeval, B., Santini, M.,
25 Schmidt, M., Shindell, D. T., Simpson, I. J., Spahni, R., Steele, L. P., Strode, S. A., Sudo, K., Szopa, S., van der Werf,
26 G. R., Voulgarakis, A., van Weele, M., Weiss, R. F., Williams, J. E., and Zeng, G.: Three decades of global methane
27 sources and sinks, *Nat. Geosci.*, 6, 813–823, <https://doi.org/10.1038/ngeo1955>, 2013.
28
29 Klusman, R. W.: Rate measurements and detection of gas microseepage to the atmosphere from an enhanced oil
30 recovery/sequestration project, Rangely, Colorado, USA. *Appl. Geochem.*, 18, 1825–1838, 2003.
31
32 Klusman, R. W.: Baseline studies of surface gas exchange and soil–gas composition in preparation for CO₂
33 sequestration research: Teapot Dome, Wyoming USA, *Am. Assoc. Pet. Geol. Bull.* 89, 981–1003, 2005.
34
35 Klusman, R. W., Leopold, M. E., and LeRoy, M. P.: Seasonal variation in methane fluxes from sedimentary basins to the
36 atmosphere: results from chamber measurements and modeling of transport from deep sources. *J. Geophys. Res.*,
37 105D, 24,661–24,670, 2000.
38
39 Kvenvolden, K. A., and Rogers, B. W.: Gaia's breathglobal methane exhalations, *Mar. Petrol. Geol.*, 22, 579–590, 2005.
40
41 Kvenvolden, K. A., and Lorenson, T. D., and Reeburgh W.: Attention turns to naturally occurring methane seepage, *EOS*
42 82, 457, 2001.
43
44 Lelieveld, J., Crutzen, P.J., and Dentener, F.J.: Changing concentration, lifetime and climate forcing of atmospheric
45 methane, *Tellus*, 50B, 128–150, 1998.
46
47 Lassey, K. R., Lowe D.C., and Smith A. M.: The atmospheric cycling of radiomethane and the “fossil fraction” of the
48 methane source, *Atmos. Chem. Phys.*, 7, 2141–2149, 2007.
49
50 LT Environmental, Inc.: Phase II raton basin gas seep investigation las animas and huerfano counties, Colorado, Project
51 #1925 oil and gas conservation response fund,
52 <http://cogcc.state.co.us/Library/Ratoasin/Phase%20II%20Seep%20Investigation%20Final%20Report.pdf>, 2007.
53
54 Maasakkers, J. D., Jacob, D. J., Sulprizio, M. P., Turner, A. J., Weitz, M., Wirth, T., Hight, C., DeFigueiredo, M., Desai
55 M., Schmeltz, R., Hockstad, L., Bloom A. A., Bowman, K. W., Seongeun, J., and Fischer, M. L.: Gridded national
56 inventory of U.S. methane emissions. *Environ. Sci. Technol.* 50, 13123–13133. doi:10.1021/acs.est.6b02878, 2016.
57
58 Mazzini, A., and Etiop, G.: Mud volcanism: an updated review, *Earth Sci. Rev.*, 168, 81–112, 2017.
59
60 McGinnis, D. F., Greinert, J., Artemov, Y., Beaubien, S. E., and Wüest, A.: Fate of rising methane bubbles in stratified
61 waters: how much methane reaches the atmosphere? *J. Geophys. Res.*, 111, C09007, 2006.
62
63 Milkov, A. V., and Etiop, G.: Revised genetic diagrams for natural gases based on a global dataset of >20,000 samples,
64 *Org. Geochem.*, in press, <https://doi.org/10.1016/j.orggeochem.2018.09.002>, 2018.



- 1
2 Milkov, A. V., Sassen, R., Apanasovich, T.V., and Dadashev, F. G.: Global gas flux from mud volcanoes: a significant
3 source of fossil methane in the atmosphere and the ocean, *Geoph. Res. Lett.*, 30, 1037, doi:10.1029/2002GL016358,
4 2003.
- 5
6 Päivi, L., Rød, J. K., and Thieme, N.: Fighting over oil: introducing a new dataset, *Conflict Management and Peace
7 Science* 24, 239-256, 2007.
- 8
9 Prather, M., et al.: Atmospheric chemistry and greenhouse gases, in climate change 2001: the scientific basis, In:
10 Houghton, J.T., Ding, Y., Griggs, D.J., Nogeur, M., van der Linden, P.J., Dai, X., Maskell, K., Johnson, C.A. (Eds.),
11 Contribution of Working Group I to the Third Assessment Report of the Intergovernmental Panel on Climate Change.
12 Cambridge University Press, Cambridge, UK, pp. 239-287, 2001.
- 13
14 Saunio, M., Bousquet, P., Poulter, B., Peregon, A., Ciais, P., Canadell, J. G., Dlugokencky, E. J., Etiope, G., Bastviken,
15 D., Houweling, S., Janssens-Maenhout, G., Tubiello, F. N., Castaldi, S., Jackson, R. B., Alexe, M., Arora, V. K., Beerling,
16 D. J., Bergamaschi, P., Blake, D. R., Brailsford, G., Bruhwiler, L., Crevoisier, C., Crill, P., Covey, K., Curry,
17 C., Frankenberg, C., Gedney, N., Höglund-Isaksson, L., Ishizawa, M., Ito, A., Joos, F., Kim, H.-S., Kleinen, T., Krummel,
18 P., Lamarque, J.-F., Langenfelds, R., Locatelli, R., Machida, T., Maksyutov, S., McDonald, K. C., Marshall, J., Melton, J.
19 R., Morino, I., Naik, V., O'Doherty, S., Parmentier, F.-J. W., Patra, P. K., Peng, C., Peng, S., Peters, G. P., Pison, I.,
20 Prigent, C., Prinn, R., Ramonet, M., Riley, W. J., Saito, M., Santini, M., Schroeder, R., Simpson, I. J., Spahni, R., Steele,
21 P., Takizawa, A., Thornton, B. F., Tian, H., Tohjima, Y., Viovy, N., Voulgarakis, A., van Weele, M., van der Werf, G. R.,
22 Weiss, R., Wiedinmyer, C., Wilton, D. J., Wiltshire, A., Worthy, D., Wunch, D., Xu, X., Yoshida, Y., Zhang, B., Zhang, Z.,
23 and Zhu, Q.: The global methane budget 2000–2012, *Earth Syst. Sci. Data*, 8, 697–751, [https://doi.org/10.5194/essd-8-
24 697-2016](https://doi.org/10.5194/essd-8-697-2016), 2016.
- 25
26 Saunio, M., Bousquet, P., Poulter, B., Peregon, A., Ciais, P., Canadell, J. G., Dlugokencky, E. J., Etiope, G., Bastviken,
27 D., Houweling, S., Janssens-Maenhout, G., Tubiello, F. N., Castaldi, S., Jackson, R. B., Alexe, M., Arora, V. K., Beerling,
28 D. J., Bergamaschi, P., Blake, D. R., Brailsford, G., Bruhwiler, L., Crevoisier, C., Crill, P., Covey, K., Frankenberg, C.,
29 Gedney, N., Höglund-Isaksson, L., Ishizawa, M., Ito, A., Joos, F., Kim, H.-S., Kleinen, T., Krummel, P., Lamarque, J.-F.,
30 Langenfelds, R., Locatelli, R., Machida, T., Maksyutov, S., Melton, J. R., Morino, I., Naik, V., O'Doherty, S., Parmentier,
31 F.-J. W., Patra, P. K., Peng, C., Peng, S., Peters, G. P., Pison, I., Prinn, R., Ramonet, M., Riley, W. J., Saito, M., Santini,
32 M., Schroeder, R., Simpson, I. J., Spahni, R., Takizawa, A., Thornton, B. F., Tian, H., Tohjima, Y., Viovy, N.,
33 Voulgarakis, A., Weiss, R., Wilton, D. J., Wiltshire, A., Worthy, D., Wunch, D., Xu, X., Yoshida, Y., Zhang, B., Zhang, Z.,
34 and Zhu, Q.: Variability and quasi-decadal changes in the methane budget over the period 2000–2012. *Atmos. Chem.
35 Phys.*, doi:10.5194/acp-2017-296, 2017.
- 36
37 Sapart, C. J., Monteil, G., Prokopiou, M., van de Wal, R. S. W., Kaplan, J. O., Sperlich, P., Krumhardt, K. M., van der
38 Veen, C., Houweling, S., Krol, M. C., Blunier, T., Sowers, T., Martinier, P., Witrant, E., Dahl-Jensen, D., and Röckmann,
39 T.: Natural and anthropogenic variations in methane sources during the past two millennia, *Nature* 490, 85–88, 2012.
- 40
41 Schwietzke, S., Sherwood, O. A., Bruhwiler, L. M. P., Miller, J. B., Etiope, G., Dlugokencky, E. J., Michel, S. E., Arling, V.
42 A., Vaughn, B. H., White, J. W. C., and Tan, P. P.: Upward revision of global fossil fuel methane emissions based on
43 isotope database, *Nature*, 538, 88-91, 2016.
- 44
45 Sciarpa, A., Cinti, D., Pizzino, L., Procesi, M., Voltattorni, N., Mecozzi, S., and Quattrocchi, F.: Geochemistry of shallow
46 aquifers and soil gas surveys in a feasibility study at the Rivara natural gas storage site (Po Plain, Northern Italy), *Appl.
47 Geochem.*, 34, 3-22, 2013.
- 48
49 Sherwood, O. A., Schwietzke, S., Arling, V. A., and Etiope, G.: Global inventory of gas geochemistry data from fossil
50 fuel, microbial and biomass burning sources, version 2017, *Earth Syst. Sci. Data*, 9, 639-656, doi:10.5194/essd-9-639-
51 2017, 2017.
- 52
53 Tang, J. H., Bao, Z. Y., Xiang, W., and Guo, Q. H.: Daily variation of natural emission of methane to the atmosphere
54 and source identification in the Luntai fault region of the Yakela condensed oil/gas field in the Tarim Basin, Xinjiang,
55 China, *Acta Geol. Sin.*, 81, 801–840, 2007.
- 56
57 Tang, J. H., Yin, H. Y., Wang, G. J., and Chen, Y. Y.: Methane microseepage from different sectors of the Yakela
58 condensed gas field in Tarim Basin, Xinjiang, China, *Appl. Geochem.*, 25, 1257–1264, 2010.
- 59
60 Tang, J., Xu, Y., Wang, G., Etiope, G., Han, W., Yao, Z., and Huang, J.: Microseepage of methane to the atmosphere
61 from the Dawanqi oil-gas field, Tarim Basin, China. *J. Geoph. Res. –Atm.*, 122, 4353-4363, 2017.
- 62
63 USGS World Energy Assessment Team: U.S. Geological Survey World Petroleum Assessment 2000, Description and
64 Results, Digital Data Series - DDS-60. U.S. Dept. of the Interior, U.S.G.S., 2000.

1
2 **Tables**3
4
5 Table 1. Parameters and data sources used to generate grid maps of geological CH₄ sources. Complete references and
6 links to data sources are provided in the Supplement.7
8
9
10
11
12
13
14
15
16
17
18
19
20
21

	Onshore seeps (OS)	Submarine seeps (SS)	Microseepage (MS)	Geothermal manifestations (GM)
Activity data	Global seep distribution (georeferenced points)	Global distribution of marine seepage zones (georeferenced areas)	Global distribution of petroleum fields (georeferenced area)	Global distribution of volcanoes and geothermal sites (georeferenced points)
<i>Data source</i>	Updated GLOGOS dataset (after CGG, 2015; Etiope, 2015)	Originally developed data-set	"Petrodata" from Päivi et al. (2007)	Global Volcanism Program (2013)
Emission factors	Measurements and estimates based on size and activity	Measurements and estimates based on size, activity and depth	- Statistical evaluation of flux data - presence of faults - seismicity	- Measurements and estimates based on size and activity - presence of sediments
<i>Data source</i>	Literature, web sources	Literature	Merged global and regional databases USGS Earthquake Lists, Maps and Statistics	Literature Sedimentary basins world map (CGG data services)
δ¹³C-CH₄	Measured or estimated value for each seep	Mean value for each seepage zone	Mean value for each basin or sub-basin	Global mean value based on statistical analysis
<i>Data source</i>	Updated GLOGOS (CGG, 2015), reservoir data (Sherwood et al. 2017) and petroleum system data (literature)	Published data or estimates based on local petroleum system	Petroleum reservoir data (Sherwood et al. 2017 and literature), seeps (OS data-set) and estimates based on the type of petroleum system	Literature data and estimates based on the type of system

15
16
17
18
19
20
21
Table 2. Estimates of global CH₄ emission from OS (onshore MV and other seeps)

	MV quiescent degassing	MV quiescent + eruption	Gas-oil seeps	Total quiescent	Total (incl. MV eruptions)
Dimitrov (2002)	0.3 – 2.6	10 - 12	nd	nd	nd
Dimitrov (2003) ^a	< 2.3	< 5	nd	nd	nd
Milkov et al (2003) ^a	< 2.9	< 6	nd	nd	nd
Etiope and Milkov (2004)	2.8 - 4	5.6 - 8	nd	nd	nd
Etiope et al (2008) ^a	< 3 - 4.5	< 6 - 9	3-4	6-8.5	9-13
Etiope et al (2011)	9	< 10-20	3-4	12-13	13-24
This work – 2827 seeps	2.83	nd	1	3.8	nd
This work – total extrapol.	~3	6.1	~ 2	~ 5	~ 8.1

nd: not determined

^a Values include shallow submarine MV, therefore they can be considered as upper limits for onshore emission.

1 Table 3. Global gridded, global extrapolated and global published geo-CH₄ emissions

2

Emission category	CH ₄ gridded emission (Tg/y)	CH ₄ extrapolated * emission (Tg/y)	Published ranges (best guess) (Tg/y)
OS - Onshore Seeps	3.8 ^{a, b}	8.1	9 – 24 ^d
SS - Submarine Seeps	3.9 ^c	5-12	10 - 30 (20) ^e
MS - Microseepage	24	24	10 – 25 ^f
GM - Geothermal Manifestations	5.7	5.7	2.2 - 7.3 ^g
Total	37.4 ^{a, b, c}	42.8 – 49.8	41- 76 (58)

3

4

5

6

7

8

9

10 Table 4. Global emission-weighted δ¹³C values (‰)

11

Emission category	Emission-weighted δ ¹³ C
OS - Onshore Seeps	-46.6
SS - Submarine Seeps	-59
MS - Microseepage	-51.4
GM - Geothermal Manifestations	-30.6
Global weighted average (based on gridded emissions, 2 nd column in Table 3)	-48.5
Global weighted average (based on globally extrapolated gridded emissions, 3 rd column in Table 3)	-49.4
Global weighted average (based on published emissions, 4 th column in Table 3)	-49.8

12

13 Table 5. Summary of uncertainty factors for the four types of geological emissions

14

Emission category /Uncertainty	Spatial distribution	Emission	δ ¹³ C
OS - Onshore Seeps	Zero uncertainty on global scale Coverage 30% gas-oil seeps (but all biggest seeps reported) Almost complete MV coverage	One order of magnitude for individual gas-oil seeps Lower uncertainty for MV (based on statistically derived emission factor and measured area)	±1‰
SS - Submarine Seepage	Zero uncertainty for central values of gridded area Area extent from published papers Unknown % of global coverage (likely >80% ?)	Published data used (central value used)	±7‰
MS - Microseepage	Theoretically predicted (measurements and process-based model) Possibility that microseepage occurs outside petroleum fields (unknown gas pools) is accounted for	< ±9 Tg/y (±38 %)	±2 ‰
GM - Geothermal Manifestations	Zero uncertainty	Theoretically assessed. Within the range of other bottom-up and process based models	±2.5‰

15

16

17

18

19

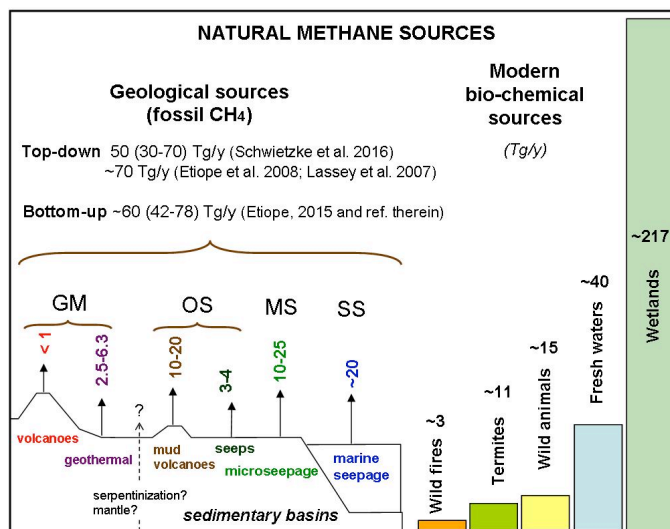
20

21

22



1



2

3

4

5

6

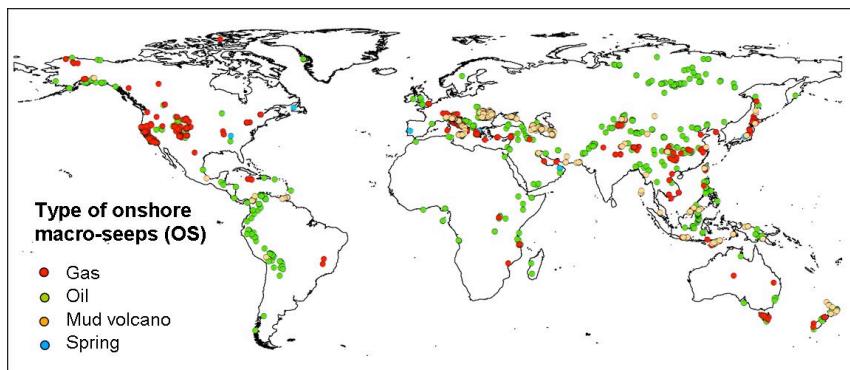
7

8

9

Fig. 1. Sketch of geo-CH₄ sources, their global emission estimates (after Etiope, 2012 and Etiope, 2015) and comparison with other natural CH₄ sources (bottom-up estimates from Kirschke et al. 2013). GM: Geothermal Manifestations, OS: Onshore Seeps, MS: Microseepage and SS: Submarine Seepage.

10



11

12

13

14

15

16

Fig. 2 Global distribution of onshore seeps (OS)

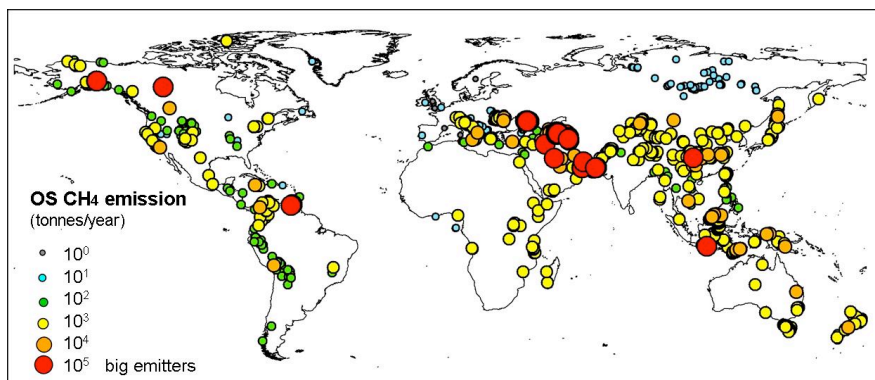


Fig. 3 Distribution of the order of magnitude of methane emission from onshore seeps.

1
2
3
4

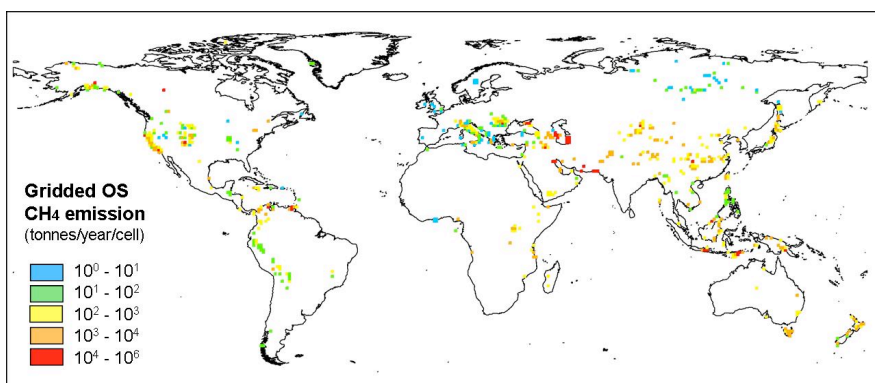


Fig. 4 Gridded map of OS methane emission. This map refers to the csv file "OS_output_2018"

5
6
7
8

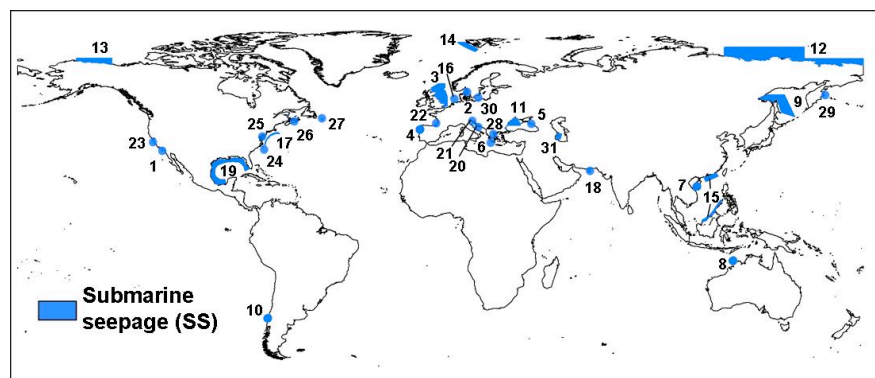
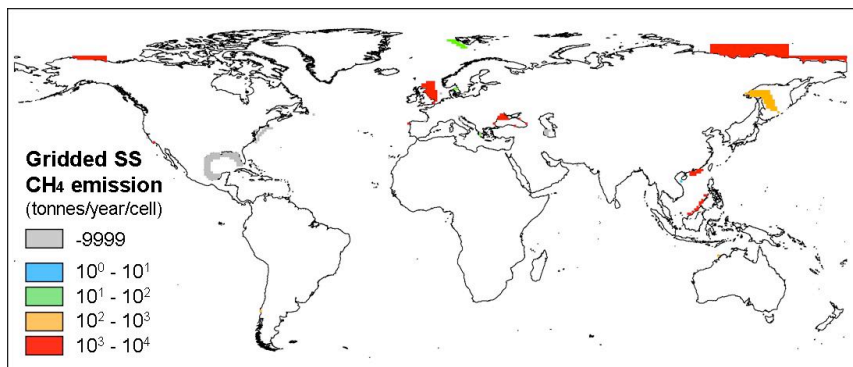


Fig. 5 Distribution of submarine seepage (SS) areas. SS numbering refers to the list in Table S4 (circle symbols mark small areas sites)

9
10
11



1



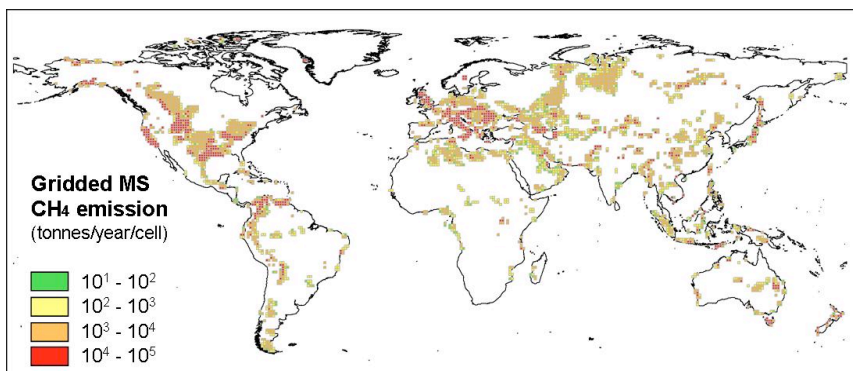
2

3

4

5

Fig. 6 Gridded map of SS methane emissions. This map refers to the csv file "SS_output"_2018.



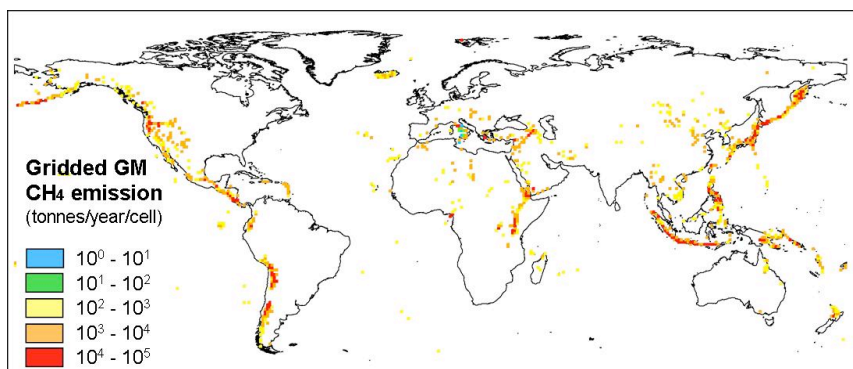
6

7

8

9

Fig. 7 Gridded map of MS methane emission. This map refers to the csv file "MS_output_2018"



10

11

12

Fig. 8 Gridded map of GM methane emission. This map refers to the csv file "GM_output_2018"



1

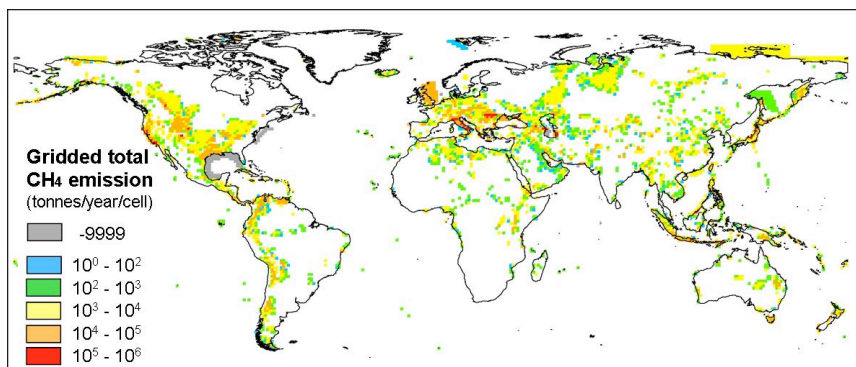


Fig. 9 Gridded map of total methane emission from OS+SS+MS+GM. This map refers to the csv file "Total geoCH4_output_2018".

2
3
4
5
6
7
8
9

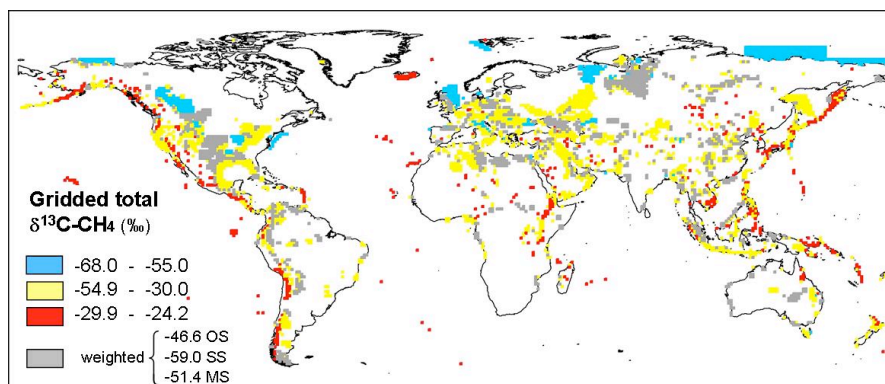


Fig. 10 Gridded map of integrated $\delta^{13}\text{C}$ values of OS+SS+MS+GM (emission-weighted within each category). "Weighted" (grey) refers to OS and MS sites where the weighted $\delta^{13}\text{C}$ value (Table 4) is used replacing -9999. This map refers to the csv file "Total geoCH4_13C_2018".

10
11
12
13
14
15
16
17
18
19